Radiative neutralino production in low energy supersymmetric models. II. The case of beam polarization

P. N. Pandita[1] and Chandradew Sharma[2]

[1]*Department of Physics, North Eastern Hill University, Shillong 793 022, India*
[2]*Department of Physics, Birla Institute of Technology and Science, Pilani—K. K. Birla Goa Campus, Goa 403 726, India*
(Received 14 October 2011; published 25 January 2012)

We study the production of the lightest neutralinos in the radiative process $e^+e^- \to \tilde{\chi}_1^0\tilde{\chi}_1^0\gamma$ in low energy supersymmetric models for the International Linear Collider energies with longitudinally polarized electron and positron beams. For this purpose we consider the case of nonminimal supersymmetric standard model as well as the case of minimal supersymmetric standard model. At the first stage of a linear collider, with $\sqrt{s} = 500$ GeV, the radiative production of the lightest neutralinos may be a viable channel to study supersymmetric partners of the standard model particles, especially if the other supersymmetric particles are too heavy to be pair produced. We consider in detail the effect of beam polarization on the production cross section. We compare and contrast the dependence of the signal cross section on the parameters of the neutralino sector of the nonminimal and minimal supersymmetric standard model when the electron and positron beams are longitudinally polarized. In order to assess the feasibility of experimentally observing the radiative neutralino production process, we consider the background to this process coming from the standard model process $e^+e^- \to \nu\bar{\nu}\gamma$ with longitudinally polarized electron and positron beams. We also consider the supersymmetric background to the radiative neutralino production process coming from the radiative production of the scalar partners of the neutrinos (sneutrinos) $e^+e^- \to \tilde{\nu}\tilde{\nu}^*\gamma$, with longitudinally polarized beams. This process can be a background to the radiative neutralino production when the sneutrinos decay invisibly.

DOI: 10.1103/PhysRevD.85.015021 PACS numbers: 11.30.Pb

I. INTRODUCTION

Supersymmetry is at present one of the most favored ideas for physics beyond the standard model (SM) [1,2]. A particularly attractive implementation of the idea of supersymmetry is the Minimal Supersymmetric standard model (MSSM) obtained by introducing the supersymmetric partners of the of the SM states, and introducing an additional Higgs doublet, with opposite hypercharge to that of the SM Higgs doublet, in order to cancel the gauge anomalies and generate masses for all the fermions of the standard model [3,4]. Supersymmetry must obviously be a broken symmetry. In order for broken supersymmetry to be effective in protecting the weak scale against large radiative corrections, the supersymmetric partners of the SM particles should have masses of the order of a few hundred GeV. Their discovery is one of the main goals of present and future accelerators. In particular, a e^+e^- linear collider with a high luminosity $\mathcal{L} = 500\ \mathrm{fb}^{-1}$, and a center-of-mass energy of $\sqrt{s} = 500$ GeV in the first stage, will be an important tool in determining the parameters of the low energy supersymmetric model with a high precision [5–9]. Furthermore, polarization of the electron (and positron) beam can enhance the capability of such a linear collider [10] in unravelling the structure of the underlying supersymmetric model.

In the minimal supersymmetric standard model the fermionic partners of the two Higgs doublets (H_1, H_2) mix with the fermionic partners of the gauge bosons to produce four neutralino states $\tilde{\chi}_i^0$, $i = 1, 2, 3, 4$, and two chargino states $\tilde{\chi}_j^{\pm}$, $j = 1, 2$. In the MSSM the lightest neutralino is favored to be the lightest supersymmetric particle, and assuming, R-parity (R_p) conservation, is absolutely stable. The neutralino states of the minimal supersymmetric standard model with R_p conservation have been studied in great detail, because the lightest neutralino, being the lightest supersymmetric particle (LSP), is the end product of any process involving supersymmetric particle in the final state.

There are alternatives to the MSSM, an elegant one being the model with an additional chiral electroweak gauge singlet Higgs superfield S which couples to the two Higgs doublet superfields H_1 and H_2 via a dimensionless trilinear term $\lambda H_1 H_2 S$ in the superpotential. This model can solve the μ problem of the MSSM in a natural manner. When the scalar component of the singlet superfield S obtains a vacuum expectation value, a bilinear term $\lambda H_1 H_2 \langle S\rangle$ involving the two Higgs doublets is naturally generated. Furthermore, when this scalar component of the chiral singlet superfield S acquires a vacuum expectation value of the order of the $SU(2)_L \times U(1)_Y$ breaking scale, it gives rise to an effective value of μ ($\mu_{\mathrm{eff}} \equiv \lambda\langle S\rangle = \lambda x$) of the order of the electroweak scale. However, the inclusion of the singlet superfield leads to additional trilinear superpotential coupling $(\kappa/3)S^3$ in the model, the so called nonminimal, or next-to-minimal [11–17], supersymmetric standard model (NMSSM). The absence of H_1H_2 term, and the absence of tadpole and mass couplings, S and S^2 in the NMSSM is made natural by postulating a suitable discrete symmetry [18,19]. The NMSSM is attractive on account of the simple resolution it offers to the μ problem, and of the scale invariance of its classical action in the supersymmetric limit [20]. Since no dimensional supersymmetric parameters are present in the superpotential of NMSSM, it is the simplest supersymmetric extension of the standard model in which the electroweak scale originates from the supersymmetry breaking scale only. Its enlarged Higgs sector may help in relaxing the fine-tuning and little hierarchy problems of the MSSM, thereby opening new perspectives for the Higgs boson searches at high energy colliders [21,22], and for dark matter searches [23]. In the nonminimal supersymmetric standard model the mixing of fermionic partners of Higgs and gauge bosons [24–26] produces five neutralino states $\tilde{\chi}_i^0$, $i = 1, 2, 3, 4, 5$, and two chargino states $\tilde{\chi}_j^{\pm}$, $j = 1, 2$. Furthermore, because of the presence of the fermionic partner of the singlet Higgs boson, the neutralino states can have an admixture of this $SU(2)_L \times U(1)_Y$ singlet fermion, thereby affecting the phenomenology of the neutralinos in the nonminimal supersymmetric standard model.

The lightest neutralino state ($\tilde{\chi}_1^0$) of MSSM or NMSSM, being typically the LSP, is stable and therefore, a possible dark matter candidate [27,28]. Since the neutralinos are among the lightest particles in low energy supersymmetric models, they are expected to be the first states to be produced at the colliding beam experiments. At an electron-positron collider, such as the International Linear Collider (ILC), the lightest neutralino can be produced in pairs

$$e^+ + e^- \longrightarrow \tilde{\chi}_1^0 + \tilde{\chi}_1^0. \tag{1.1}$$

This process proceeds via Z boson and selectron exchange [29,30]. In collider experiments the lightest neutralino escapes detection. In such a situation the production of the lightest neutralino pair (1.1) is invisible. Therefore, we must look for the signature of neutralinos in the radiative process

$$e^- + e^+ \longrightarrow \tilde{\chi}_1^0 + \tilde{\chi}_1^0 + \gamma. \tag{1.2}$$

Despite this process being suppressed by the square of the electromagnetic coupling, it might be the first process where the lightest supersymmetric states could be observed at the e^+e^- colliders. The signal of the radiative process (1.2) is a single high energy photon with the missing energy carried away by the neutralinos. The process (1.2) has been studied in detail in the minimal supersymmetric standard model [31–41]. Some of these studies underline the importance of longitudinal [39], and even transverse beam polarizations. On the other hand, the signature "photon plus missing energy," that arises in the process (1.2) has been studied in detail by different LEP collaborations [42–46]. Furthermore, the radiative neutrino process $e^+e^- \to \nu\bar{\nu}\gamma$ in the SM is the leading process with this signature, for which the cross section depends on the number N_ν of light neutrino species [47]. The LEP collaborations have found no deviations from the SM prediction, and, therefore, only bounds on the masses of supersymmetric particles have been set [42–44,46]. For a review of the experimental situation, see Ref. [48].

Most of the theoretical studies on radiative neutralino production in the literature have been carried out in the framework of the minimal supersymmetric standard model. This includes calculations relevant to ILC with a high center-of-mass energy, high luminosity and longitudinally polarized beams, as well as study of the SM background from the radiative neutrino production

$$e^+e^- \longrightarrow \nu + \bar{\nu} + \gamma, \tag{1.3}$$

and the supersymmetric background from radiative sneutrino production

$$e^+e^- \longrightarrow \tilde{\nu} + \tilde{\nu}^* + \gamma. \tag{1.4}$$

The discovery potential of ILC may be significantly enhanced [49] if both beams are polarized, particularly if other SUSY states like heavier neutralino, chargino or even slepton pairs are too heavy to be produced at the first stage of the ILC at $\sqrt{s} = 500$ GeV.

In a previous paper (referred to as paper I) we have carried out a detailed study of the radiative process (1.2) in the nonminimal supersymmetric model and compared the predictions with those of the minimal supersymmetric standard model [50]. This study was carried out for unpolarized electron and positron beams. In this paper we continue this study and consider the radiative process (1.2) in the nonminimal supersymmetric standard model with polarized electron and positron beams to understand in detail if the signal can be enhanced by the use of polarized beams. Furthermore, the SM background photons from radiative neutrino production process (1.3) with beam polarizations will have to be taken into account for a proper analysis of the radiative neutralino production process (1.2). Beam polarizations could enhance the signal photons for the process (1.2) for NMSSM and reduce those from the SM background at the same time, which could lead to the enhancement of the statistics. We will also consider supersymmetric background photons from radiative sneutrino production process (1.4) with polarized beams. This is important if sneutrino production is kinematically accessible and if the sneutrino decay is invisible. We will compare and contrast the results obtained for NMSSM with those for the minimal supersymmetric standard model with polarized beams. This will include the signal for the radiative neutralino process, and the dependence of the cross sections on the parameters of the neutralino sector. This comparison will allow us to assess the feasibility of observing the radiative neutralino process for the most popular low energy supersymmetric models at a e^+e^- collider.

The plan of the paper is as follows. In Sec. II, we calculate the cross section for the signal process (1.2) in the nonminimal supersymmetric standard model, and compare it with the corresponding cross section in the minimal supersymmetric standard model, for unpolarized and polarized electron and positron beams. In order to calculate the cross section in the NMSSM, we fix the parameter space that we use in our calculations. This is done by using various theoretical and experimental constraints on the parameter space of NMSSM. In particular, we constrain the values of the trilinear superpotential parameters λ and κ which enter the neutralino mass matrix of the NMSSM. We also describe the phase space for the signal process as well as the cuts on outgoing photon angle and energy that we use to regularize the infrared and collinear divergences in the tree-level cross section. We then analyze numerically the dependence of the cross section on the parameters of the neutralino sector, and on the selectron masses, for unpolarized and polarized beams. Here we also calculate the photon energy distribution for the radiative production of the second lightest neutralino in the NMSSM and compare it with the corresponding distribution for the lightest neutralino for unpolarized and polarized beams, respectively.

In Sec. III we analyze the backgrounds to the radiative neutralino process (1.2) with polarized beams. This includes the background from SM process (1.3), as well as from the supersymmetric process (1.4) for the case of polarized beams. In Sec. IV we study in detail the beam polarization dependence of the cross section for the radiative neutralino production process as well as for the backgrounds processes. Here we also consider the statistical significance for measuring the excess of photons from radiative neutralino production over the backgrounds, and calculate this quantity for NMSSM, and compare it with the corresponding results in MSSM. We summarize our results and conclusions in Sec. V. Our notations and results on the neutralino mass matrices and couplings are summarized in Appendix .

II. RADIATIVE NEUTRALINO PRODUCTION

The Feynman diagrams for the radiative process

$$e^-(p_1) + e^+(p_2) \rightarrow \tilde{\chi}_1^0(k_1) + \tilde{\chi}_1^0(k_2) + \gamma(q), \qquad (2.1)$$

are shown in Fig. 1, where the symbols in the brackets denote the four momenta of the respective particles. In NMSSM, and in MSSM, this process proceeds at the tree level via t- and u-channel exchange of right and left selectrons $\tilde{e}_{R,L}$, and via Z boson exchange in the s channel. In order to calculate the cross section for the radiative production of neutralinos we need to compute the couplings of the neutralinos to electrons, to the scalar partners of electrons, the selectrons, and to Z^0 bosons. We summarize these couplings for MSSM and NMSSM [51,52] in Appendix . As can be seen in Appendix , the couplings of the lightest neutralino are determined by the corresponding elements of the neutralino mixing matrix (N_{ij} or N'_{ij}). For numerical calculation of the radiative neutralino cross section in the MSSM, we have chosen to work with the parameters in the Snowmass Points and Slopes (SPS 1a) scenario [53]. The parameters of the SPS 1a scenario are summarized in Table I. However, since in the SPS 1a scenario the value of the parameters μ and M_2 are fixed, we shall use a different set of parameters to study the dependence of the neutralino mass and the radiative neutralino production cross section on μ and M_2, and on the selectron masses. This set of parameters is shown in Table II. We shall call this set of parameters as the MSSM electroweak symmetry breaking scenario (EWSB) [54]. As in paper I, for the NMSSM we use a set of parameters that is obtained by imposing theoretical and experimental constraints on the parameter space of the NMSSM. The parameters that enter the neutralino mass matrix of the NMSSM are, apart from M_1 and M_2, $\tan\beta$, $\mu(\equiv \lambda\langle S\rangle = \lambda x)$, λ and κ. For M_1, M_2 and M_3 we use the values which are consistent with the usual GUT relation $M_1/\alpha_1 = M_2/\alpha_2 = M_3/\alpha_3$. We note that for the MSSM in SPS 1a scenario, the value of the parameter $\tan\beta = 10$. In order to remain close to the SPS 1a scenario of MSSM, we have chosen for our numerical calculations in NMSSM values of $\tan\beta = 10$, whereas the rest of the parameters are chosen in such a way that the lightest Higgs boson mass, the lightest neutralino mass and the lightest chargino mass satisfy the present experimental lower limits. We have also imposed on the parameter space of NMSSM, the theoretical constraint that there is no charge and color breaking global minimum of the scalar potential, and that a Landau pole does not develop below the grand unified scale ($M_{\rm GUT} \approx 10^{16}$ GeV). The consequence of imposing these constraints on the parameter space of NMSSM, and the resulting masses for various particles for a particular choice of input parameters is summarized in Table III. Since the neutralino mass matrix depends on the parameters λ and κ, it is useful to study the possible values of these parameters, with all other parameters fixed, which satisfy the phenomenological and theoretical constraints discussed above. In Fig. 2 we show a plot of λ versus κ, with all other input parameters fixed as in Table III, and with the lightest neutralino, the lightest Higgs boson, and the lightest chargino masses as in Table III with a variation of less than 5%. Figure 2 shows the range of λ and κ values that are consistent with all the constraints discussed above for the set of input parameters in Table III. We note that for the set of input values in Table III, values of $\lambda \lesssim 0.4$, with $\kappa \lesssim 0.22$, lead to an

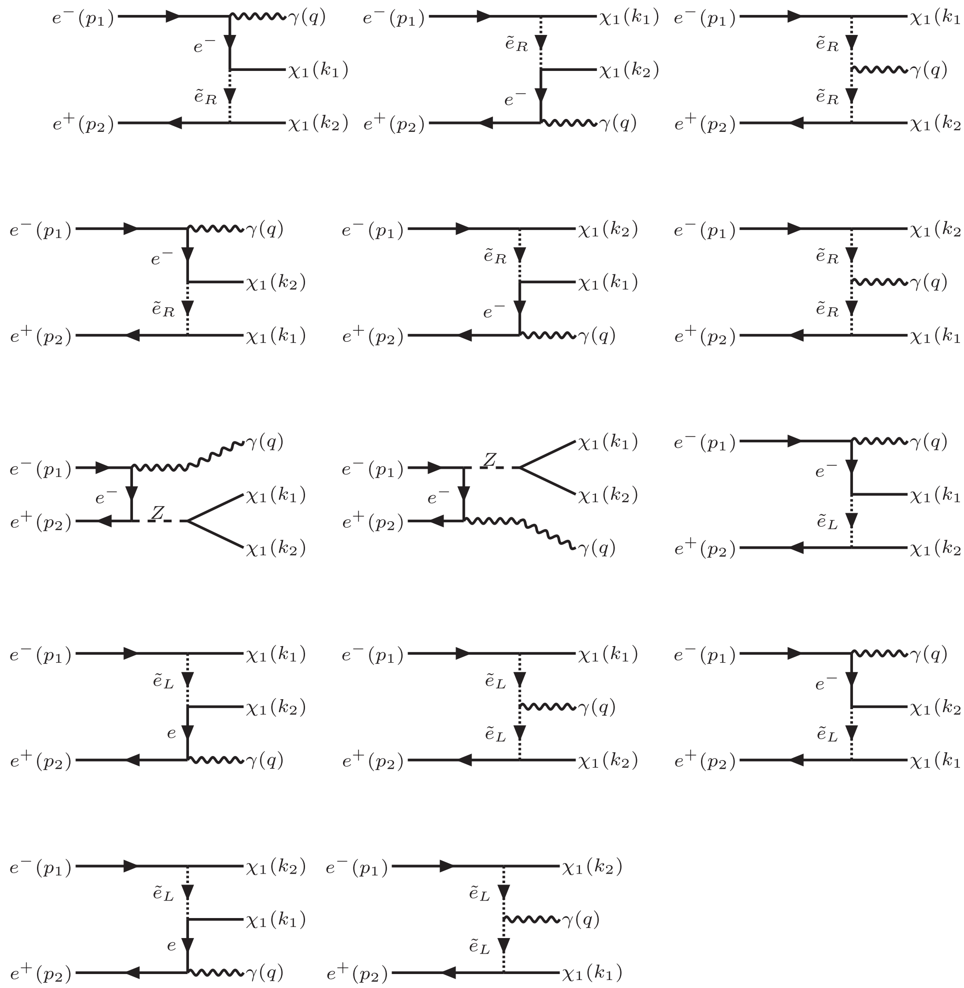

FIG. 1. Feynman diagrams for the radiative production of lightest neutralinos in the process $e^+e^- \to \tilde{\chi}_1^0\tilde{\chi}_1^0\gamma$.

unphysical global minimum. On the other hand, values of $\lambda \gtrsim 0.57$, with $\kappa \gtrsim 0.45$, lead to a Landau pole below the GUT scale. Thus, the allowed values of λ and κ, for the given set of input parameters, and for the fixed masses of lightest neutralino, the lightest Higgs boson, and the lightest chargino, as in Table III, lie in a narrow range $0.4 \lesssim \lambda \lesssim 0.57$ for $0.22 \lesssim \kappa \lesssim 0.45$. For definiteness, we have chosen to work with the values of $\lambda = 0.54$ and $\kappa = 0.45$ in this paper. These values correspond to the peak in the λ versus κ plot in Fig. 2. For the parameters of Table III, the composition of the lightest neutralino in NMSSM is given by

$$N'_{1j} = (0.48, -0.23, 0.57, -0.55, 0.30). \tag{2.2}$$

TABLE I. Input parameters and resulting masses for various states in the MSSM SPS 1a scenario.

$\tan\beta = 10$	$Q = 100$ GeV	$m_{1/2} = 250$ GeV	$m_0 = 100$ GeV	$A_0 = -100$ GeV
$m_{\chi_1^0} = 97$ GeV	$m_{\chi_1^\pm} = 180$ GeV	$m_{\tilde{e}_R} = 136$ GeV	$m_{\tilde{\nu}_e} = 185$ GeV	$m_h = 110$ GeV
$m_{\chi_2^0} = 180$ GeV	$m_{\chi_2^\pm} = 379$ GeV	$m_{\tilde{e}_L} = 195$ GeV	$m_H = 396$ GeV	$m_A = 395$ GeV

TABLE II. Input parameters and resulting masses of various states in MSSM EWSB scenario.

$\tan\beta = 10$	$\mu = 149$ GeV	$M_1 = 150$ GeV	$M_2 = 300$ GeV	$M_3 = 1050$ GeV
$M_A = 242$ GeV	$A_t = 3000$ GeV	$A_b = 3000$ GeV	$A_\tau = 1000$ GeV	
$m_{\chi_1^0} = 108$ GeV	$m_{\chi_1^\pm} = 135$ GeV	$m_{\tilde{e}_R} = 137$ GeV	$m_{\tilde{\nu}_e} = 187$ GeV	$m_h = 118$ GeV
$m_{\chi_2^0} = -160$ GeV	$m_{\chi_2^\pm} = 328$ GeV	$m_{\tilde{e}_L} = 197$ GeV	$m_H = 243$ GeV	$m_A = 242$ GeV

TABLE III. Input parameters and resulting masses of various states in NMSSM.

$\tan\beta = 10$	$\mu = 149$ GeV	$M_1 = 150$ GeV	$M_2 = 300$ GeV	$M_3 = 1050$ GeV
$M_A = 242$ GeV	$A_t = 3000$ GeV	$A_b = 3000$ GeV	$A_\tau = 1000$ GeV	$\lambda = 0.54$
$\kappa = 0.45$	$A_\lambda = 880$ GeV	$A_\kappa = 10$ GeV	$m_{\tilde{e}_R} = 137$ GeV	$m_{\tilde{e}_L} = 197$ GeV
$m_{\chi_1^0} = 94$ GeV	$m_{\chi_1^\pm} = 135$ GeV	$m_{\tilde{\nu}_e} = 187$ GeV	$m_h = 122$ GeV	
$m_{\chi_2^0} = -160$ GeV	$m_{\chi_2^\pm} = 328$ GeV	$m_{H_2} = 242$ GeV	$m_{H_3} = 1313$ GeV	

From the composition (2.2), we see that the lightest neutralino has a sizable singlet component, thereby changing the neutralino phenomenology in the NMSSM as compared to MSSM. For comparison, we also show the particle content of the lightest neutralino in MSSM

$$N_{1j} = (0.6, -0.21, 0.61, -0.47), \tag{2.3}$$

for the parameter set in Table II. In Fig. 3(a) we have plotted the constant contour plots for the mass of lightest neutralino in NMSSM in the μ-M_2 plane. We emphasize that the choice of μ and M_2 values in this plot have been taken to be consistent with phenomenological and theoretical constraints as described above. For comparison, we have also plotted the corresponding contour plots for MSSM in Fig. 3(b) with parameters as in Table II.

A. Cross section for the signal process

In NMSSM, and in MSSM, the process (2.1) proceeds at the tree level via t- and u-channel exchange of right and left selectrons $\tilde{e}_{R,L}$, and via Z boson exchange in the s channel. The photon is radiated off the incoming beams or the exchanged selectrons. The corresponding Feynman diagrams are shown in Fig. 1. The differential cross section for (2.1) can be written as [33,55]

$$d\sigma = \frac{1}{2}\frac{(2\pi)^4}{2s}\prod_f \frac{d^3\mathbf{p}_f}{(2\pi)^3 2E_f}\delta^{(4)} \times (p_1 + p_2 - k_1 - k_2 - q)|\mathcal{M}|^2, \tag{2.4}$$

where $\mathbf{p}_f$ and E_f denote the final three-momenta $\mathbf{k}_1$, $\mathbf{k}_2$, $\mathbf{q}$ and the final energies E_{χ_1}, E_{χ_2}, and E_γ of the neutralinos and the photon, respectively. The squared matrix element $|\mathcal{M}|^2$ in (2.4) can be written as [33]

$$|\mathcal{M}|^2 = \sum_{i\le j} T_{ij}, \tag{2.5}$$

where T_{ij} are squared amplitudes corresponding to the Feynman diagrams in Fig. 1. A sum over the spins of the outgoing neutralinos, as well as a sum over the polarizations of the outgoing photon is included in T_{ij}. We have included the longitudinal beam polarizations of electrons, P_{e^-}, and positrons, P_{e^+}, with $-1 \le P_{e^\pm} \le +1$, while calculating the cross section for the radiative neutralino production process. The phase space in (2.4) described in [33].

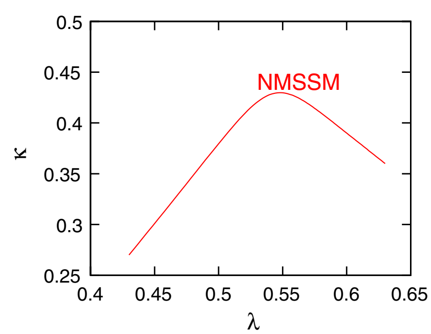

FIG. 2 (color online). Plot of λ versus κ for the set of input parameters in Table III.

1. Numerical results

We have calculated the squared amplitudes and the tree-level cross section for radiative neutralino production (1.2), and the background from radiative neutrino and

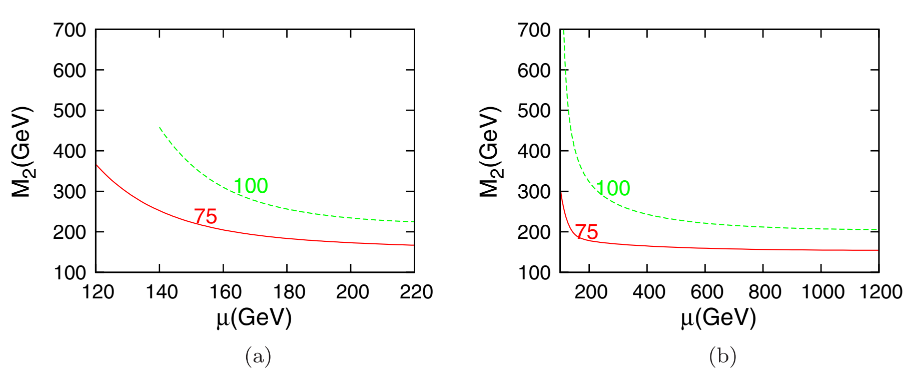

FIG. 3 (color online). (a) Contour plots of constant lightest neutralino mass $m_{\chi_1^0}$ in μ-M_2 plane for NMSSM; (b) for MSSM.

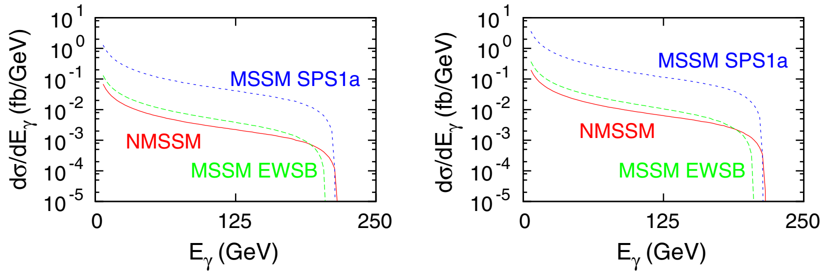

(a) (b)

FIG. 4 (color online). (a) Photon energy distribution $\frac{d\sigma}{dE_\gamma}$ for the radiative neutralino production for NMSSM (red solid line), for MSSM EWSB (green dashed line) and MSSM SPS 1a (blue dashed line) at $\sqrt{s} = 500$ GeV with $(P_{e^-}, P_{e^+}) = (0, 0)$; (b) with $(P_{e^-}, P_{e^+}) = (0.8, -0.6)$.

sneutrino production, (1.3) and (1.4), with polarized electron and positron beams, using the program CALCHEP [54]. We note that when integrating the squared amplitude for the radiative neutralino production, the $s - t$ interference terms cancel the $s - u$ interference terms due to a symmetry in these channels, due to the Majorana properties of the neutralinos [39]. The tree level cross sections have infrared and collinear divergences, which need to be regularized [33]. To do this we define the fraction of the beam energy carried by the photon as $x = E_\gamma/E_{\rm beam}$, where $\sqrt{s} = 2E_{\rm beam}$ is the center-of-mass energy, and E_γ is the energy carried away by the photon. We then impose the following cuts on x, and on the scattering angle θ_γ of the photon [49]:

$$0.02 \le x \le 1 - \frac{m^2_{\chi^0_1}}{E^2_{\rm beam}}, \tag{2.6}$$

$$-0.99 \le \cos\theta_\gamma \le 0.99. \tag{2.7}$$

The lower limit on x in (2.6) corresponds to a photon energy $E_\gamma = 5$ GeV for the center of mass energy $\sqrt{s} = 500$ GeV. The upper limit of $(1 - m^2_{\chi^0_1}/E^2_{\rm beam})$ on x corresponds to the maximum energy that a photon can carry in radiative neutralino production.

In order to implement the cuts on the photon energy in the calculation of the cross sections, we have taken the mass of the lightest neutralino in NMSSM to be $m_{\chi^0_1} = 94$ GeV for the parameter set shown in Table III. For MSSM SPS1a, we take $m_{\chi^0_1} = 97$ GeV and for MSSM EWSB $m_{\chi^0_1} = 108$ GeV.

We note that for values of $\sqrt{s} = 500$ GeV, and for $m_{\chi^0_1} \ge 94$ GeV, this cut reduces a substantial amount of the on-shell Z boson contribution to radiative neutrino production process.

2. Photon energy (E_γ) distribution and total beam energy ($\sqrt{s}$) dependence

Using the procedure described above, we have calculated the energy distribution of the photons from radiative neutralino production in NMSSM, in MSSM SPS 1a, and in MSSM EWSB for both unpolarized and polarized electron and positron beams, respectively. These are shown in Fig. 4, where we compare the energy distribution of the photons in these models. In Fig. 5 we show the total beam energy $\sqrt{s}$ dependence of the cross sections for NMSSM, and for MSSM EWSB and MSSM SPS 1a, respectively. We note that the photon energy distribution and the total cross section for radiative neutralino production in NMSSM and in MSSM EWSB are very close to each other,

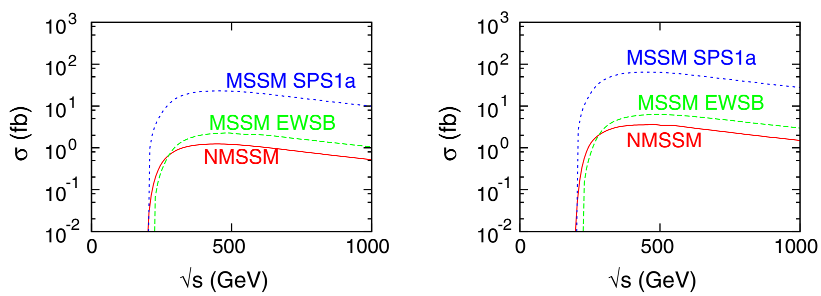

(a) (b)

FIG. 5 (color online). (a) Total energy $\sqrt{s}$ dependence of the cross sections σ for radiative neutralino production $e^+e^- \to \tilde\chi^0_1\tilde\chi^0_1\gamma$ for NMSSM (red solid line) and for MSSM EWSB scenario (green dashed line) and MSSM SPS 1a (blue dashed line) with $(P_{e^-}, P_{e^+}) = (0, 0)$, (b) with $(P_{e^-}, P_{e^+}) = (0.8, -0.6)$.

and are smaller as compared to what one obtains in MSSM SPS 1a scenario.

3. Dependence on μ and M_2

Since the neutralino mass matrix, and hence the lightest neutralino mass, depends on μ and M_2, it is important to study the dependence of the radiative neutralino cross section on these parameters. In the nonminimal supersymmetric standard model, $\mu(\equiv \lambda\langle S\rangle = \lambda x)$ and M_2 are independent parameters. We have, therefore, studied the cross section $\sigma(e^+e^- \to \tilde{\chi}_1^0\tilde{\chi}_1^0\gamma)$ as a function of μ and M_2 independently. In Fig. 6 we show the μ dependence of the total cross section for the radiative production of neutralinos for NMSSM as well as MSSM EWSB. We recall that in the MSSM SPS 1a scenario these parameters are fixed. As is seen from Fig. 6, the total cross section increases with μ. The plot of total cross section versus μ in Fig. 6 is plotted in the range $\mu \in [120, 170]$ GeV in NMSSM and in MSSM EWSB. Note that the parameter values are chosen so as to avoid color and charge breaking minima, absence of Landau pole, and the phenomenological constraints on different particle masses. Furthermore, in Fig. 7 we show the M_2 dependence of the total cross section for radiative neutralino production for NMSSM and MSSM EWSB. The total cross section decreases with increasing value of M_2. The graph of total cross section versus M_2 in Fig. 7 is plotted for the interval $M_2 \in [150, 450]$ GeV in NMSSM and in MSSM EWSB so as to satisfy the theoretical and phenomenological constraints described above. From Figs. 6 and 7 we note that the cross section is significantly enhanced when the electron and positron beams are polarized as compared to the case when the beams are unpolarized.

4. Dependence on selectron masses

The cross section for radiative neutralino production $\sigma(e^+e^- \to \tilde{\chi}_1^0\tilde{\chi}_1^0\gamma)$ proceeds mainly via right and left selectron $\tilde{e}_{R,L}$ exchange in the t and u channels. In the NMSSM and MSSM EWSB, the selectron masses are independent parameters. In Fig. 8 and 9 we show the dependence of total cross section of radiative neutralino production on the left and right selectron masses. The cross section is not very sensitive to the selectron masses for both models. Furthermore, the total neutralino production cross section is smaller in NMSSM as compared to MSSM EWSB as a function of left as well as right selectron masses. Again we note that the cross sections, as a function of selectron masses, are larger in the case of polarized beams as compared to the unpolarized case.

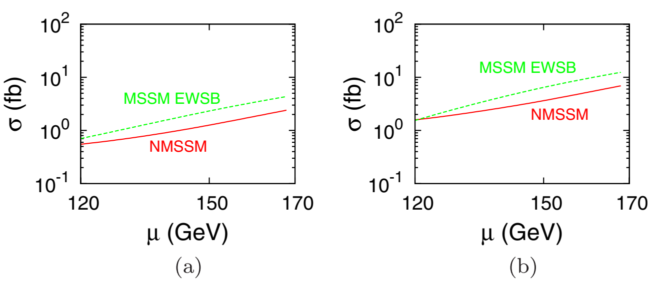

FIG. 6 (color online). (a) Total cross section σ for the radiative neutralino production versus μ for NMSSM (red solid line) and for MSSM EWSB scenario (green dashed) at $\sqrt{s} = 500$ GeV with $(P_{e^-}, P_{e^+}) = (0, 0)$; (b) with $(P_{e^-}, P_{e^+}) = (0.8, -0.6)$.

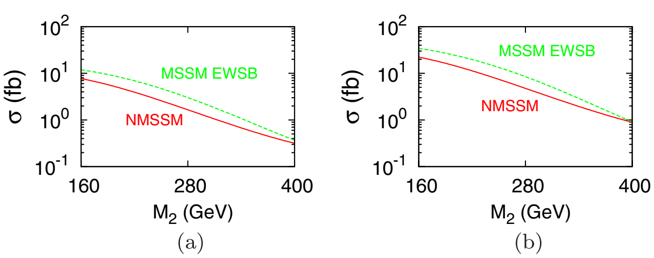

FIG. 7 (color online). (a) Total cross section σ for the radiative neutralino production versus M_2 for NMSSM (red solid line) and for MSSM EWSB scenario (green dashed) at $\sqrt{s} = 500$ GeV with $(P_e^-, P_e^+) = (0, 0)$; (b) with $(P_{e^-}, P_{e^+}) = (0.8, -0.6)$.

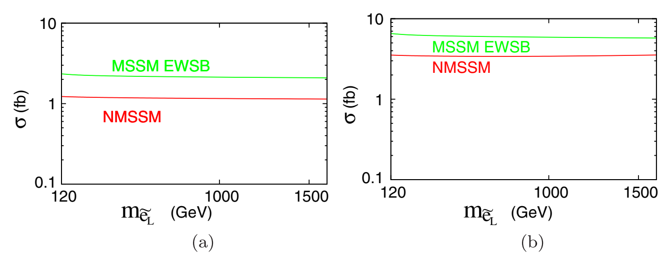

FIG. 8 (color online). (a) Total cross section σ for the radiative neutralino production versus $m_{\tilde{e}_L}$ for NMSSM (red solid line) and for MSSM in the EWSB scenario (green dashed) at $\sqrt{s} = 500$ GeV with $(P_{e^-}, P_{e^+}) = (0, 0)$, (b) with $(P_{e^-}, P_{e^+}) = (0.8, -0.6)$.

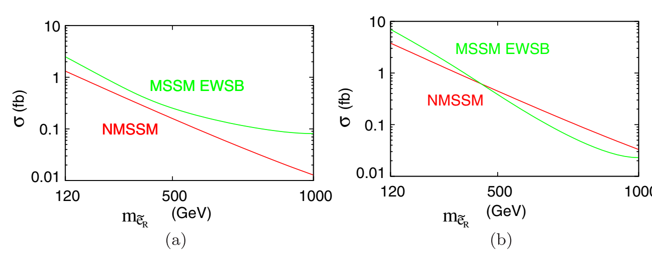

FIG. 9 (color online). (a) Total cross section σ for the radiative neutralino production versus $m_{\tilde{e}_R}$ for NMSSM (red solid line) and for MSSM in the EWSB scenario (green dashed) at $\sqrt{s} = 500$ GeV with $(P_{e^-}, P_e^+) = (0, 0)$, (b) with $(P_{e^-}, P_{e^+}) = (0.8, -0.6)$.

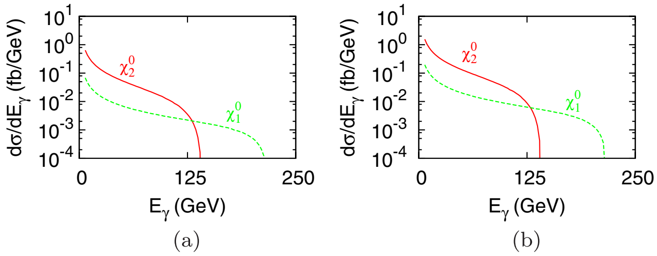

FIG. 10 (color online). (a) Photon energy distribution $\frac{d\sigma}{dE_\gamma}$ for the radiative production of second lightest neutralino in NMSSM (red solid line), and the lightest neutralino for NMSSM (green dashed line) at $\sqrt{s} = 500$ GeV with $(P_{e^-}, P_{e^+}) = (0, 0)$; (b) with $(P_{e^-}, P_{e^+}) = (0.8, -0.6)$.

5. Photon energy (E_γ) distribution for the production of the second lightest neutralino

The cross section for the production of the lightest neutralino in NMSSM is relatively small compared with the corresponding cross section for the lightest neutralino in the MSSM SPS1a. It may, therefore, be useful to consider the radiative production of the second lightest neutralino in the NMSSM. For the parameter set of Table III the composition of the second lightest neutralino in NMSSM is given by

$$N'_{2j} = (0.87, 0.21, -0.22, 0.34, -0.19). \tag{2.8}$$

We have calculated the photon energy distribution for the radiative production of the second lightest neutralino in NMSSM for the set of parameters shown in Table III. This is shown in Fig. 10. For comparison we have also shown the photon energy distribution for the radiative production of the lightest neutralino in NMSSM. We see that the cross section for the production of the second lightest neutralino is much smaller than the cross section for the lightest neutralino at photon energy greater than 140 GeV. However, at lower photon energies the photon energy distribution for the second lightest neutralino is significantly larger, both for unpolarized as well as polarized beams.

III. BACKGROUND PROCESSES

A. The neutrino background

The major background to the radiative neutralino production (2.1) comes from the SM radiative neutrino production process [40,47,56–58]

$$e^+ + e^- \to \nu_\ell + \bar{\nu}_\ell + \gamma, \qquad \ell = e, \mu, \tau. \tag{3.1}$$

In this process ν_e are produced via t-channel W boson exchange, and $\nu_{e,\mu,\tau}$ via s-channel Z boson exchange. We Feynman diagrams contributing to the process (3.1) are shown in Fig. 11.

The background photon energy distribution $\frac{d\sigma}{dE_\gamma}$ and $\sqrt{s}$ dependence of the cross section σ for radiative neutrino production $e^+e^- \to \nu\bar{\nu}\gamma$ with polarized electron and positron beams is the same for both NMSSM and MSSM. As shown in Fig. 12 the photon energy distribution from the radiative neutrino production peaks at $E_\gamma = (s - m_Z^2)/(2\sqrt{s}) \approx 242$ GeV because of the radiative Z production ($\sqrt{s} > m_Z$). This photon background from radiative neutrino production can be reduced by imposing an upper cut on the photon energy $x^{\max} = E_\gamma^{\max}/E_{\text{beam}} = 1 - m_{\chi_1^0}^2/E_{\text{beam}}^2$ GeV in NMSSM, see Eq. (2.6), which is the kinematical endpoint $E_\gamma^{\max} \approx 215$ GeV of the energy distribution of the photon from radiative neutralino production

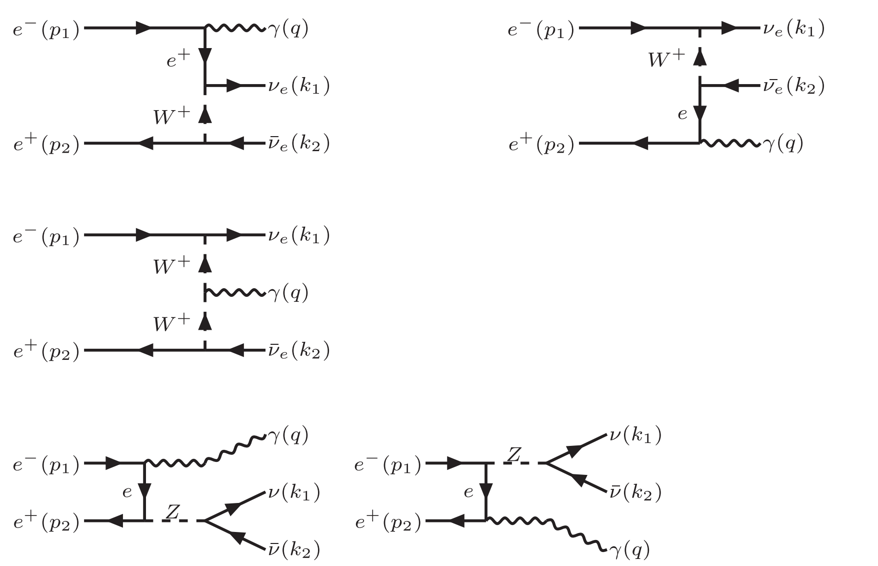

FIG. 11. Feynman diagrams contributing to the radiative neutrino process $e^+e^- \to \nu\bar{\nu}\gamma$.

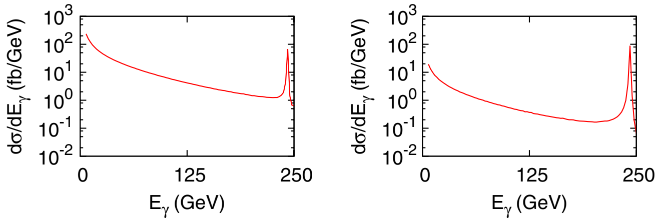

(a) (b)

FIG. 12 (color online). (a) The photon energy distribution $\frac{d\sigma}{dE_\gamma}$ for the radiative neutrino process $e^+e^- \rightarrow \nu\bar{\nu}\gamma$ at $\sqrt{s} = 500$ GeV with $(P_{e^-}, P_e^+) = (0, 0)$, (b) with $(P_{e^-}, P_{e^+}) = (0.8, -0.6)$.

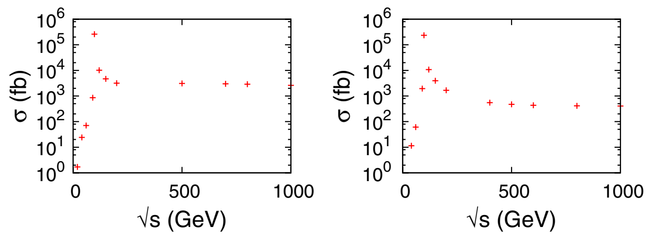

(a) (b)

FIG. 13 (color online). (a) Total energy $\sqrt{s}$ dependence of the cross sections σ for radiative neutrino cross section $\sigma(e^+e^- \rightarrow \nu\bar{\nu}\gamma)$ with $(P_{e^-}, P_{e^+}) = (0, 0)$, (b) with $(P_{e^-}, P_{e^+}) = (0.8, -0.6)$.

$$m^2_{\tilde{\chi}^0_1} = \frac{1}{4}(s - 2\sqrt{s}E^{\max}_\gamma). \tag{3.2}$$

In order to achieve this, one would have to separate the signal and background processes. This would be possible if the neutralino is heavy enough, such that the endpoint is removed from the Z^0 peak of the background distribution. See also [49]. In Fig. 13 we show the $\sqrt{s}$ dependence of the total radiative neutrino cross section with unpolarized and polarized electron and positron beams without imposing upper cut on the photon energy. In Section IV the upper cut on the photon energy $E^{\max}_\gamma = 214.7$ GeV is used for the calculation of cross section for the radiative neutrino production.

B. The supersymmetric background

Apart from the SM background coming from (3.1), the radiative neutralino production (2.1) has a background coming from the supersymmetric sneutrino production process [40,59]

$$e^+ + e^- \rightarrow \tilde{\nu}_\ell + \tilde{\nu}^*_\ell + \gamma, \qquad \ell = e, \mu, \tau. \tag{3.3}$$

The lowest order Feynman diagrams contributing to the process (3.3) are shown in Fig. 14. This process receives t-channel contributions via virtual charginos for $\tilde{\nu}_e\tilde{\nu}^*_e$ production, as well as s-channel contributions from Z boson exchange for $\tilde{\nu}_{e,\mu,\tau}\tilde{\nu}^*_{e,\mu,\tau}$ production. In Fig. 15, we show the photon energy distribution $\frac{d\sigma}{dE_\gamma}$ for radiative sneutrino production $e^+e^- \rightarrow \tilde{\nu}\tilde{\nu}^*\gamma$ at $\sqrt{s} = 500$ GeV with unpolarized and longitudinally polarized electron and positron beams. The corresponding total cross section for the radiative sneutrino production is shown in Fig. 16.

Radiative sneutrino production (3.3) can be a major supersymmetric background to neutralino production (2.1) if sneutrinos decay mainly invisibly, e.g. via $\tilde{\nu} \rightarrow \tilde{\chi}^0_1\nu$. This leads to so called "virtual LSP" scenario [40]. However, if kinematically allowed, other visible decay channels like $\tilde{\nu} \rightarrow \tilde{\chi}^\pm_1\ell^\mp$ reduce the background rate from radiative sneutrino production. For example in the SPS 1a scenario [53,60] of the MSSM we have $\mathrm{BR}(\tilde{\nu}_e \rightarrow \tilde{\chi}^0_1\nu_e) = 85\%$.

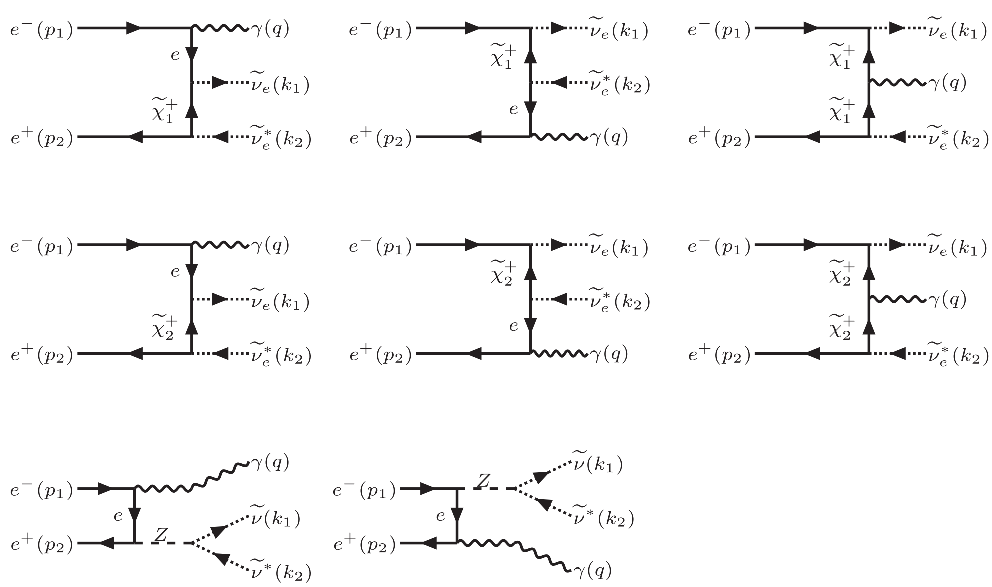

FIG. 14. Feynman diagrams contributing to the radiative sneutrino production process $e^+e^- \rightarrow \tilde{\nu}\tilde{\nu}^*\gamma$.

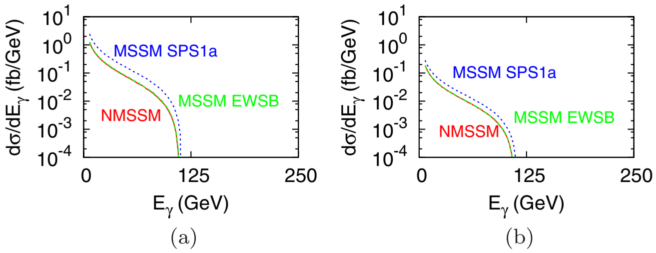

FIG. 15 (color online). (a) The photon energy distribution $\frac{d\sigma}{dE_\gamma}$ for the radiative sneutrino production $e^+e^- \to \tilde{\nu}\tilde{\nu}^*\gamma$ at $\sqrt{s} = 500$ GeV with $(P_{e^-}, P_e^+) = (0, 0)$, (b) with $(P_{e^-}, P_{e^+}) = (0.8, -0.6)$.

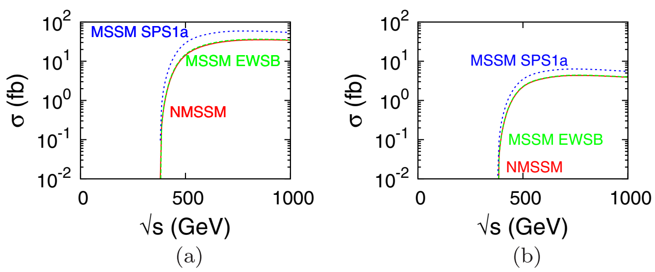

FIG. 16 (color online). (a) Total energy $\sqrt{s}$ dependence of the radiative sneutrino production cross section $\sigma(e^+e^- \to \tilde{\nu}\tilde{\nu}^*\gamma)$ with $(P_{e^-}, P_{e^+}) = (0, 0)$, (b) with $(P_{e^-}, P_{e^+}) = (0.8, -0.6)$.

Furthermore, neutralino production $e^+e^- \to \tilde{\chi}_1^0\tilde{\chi}_2^0$ followed by subsequent radiative neutralino decay [61] $\tilde{\chi}_2^0 \to \tilde{\chi}_1^0\gamma$ is also a potential background. However, significant branching ratios $\mathrm{BR}(\tilde{\chi}_2^0 \to \tilde{\chi}_1^0\gamma) > 10\%$ are obtained only for small values of $\tan\beta < 5$ and/or $M_1 \sim M_2$ [41,62,63]. Thus, we neglect this background, detailed discussions of which can be found in Refs. [62–64].

IV. THE EFFECT OF LONGITUDINAL BEAM POLARIZATION

In this Section we study in detail the effect of longitudinal beam polarization on the cross section for radiative neutralino production in NMSSM, and MSSM, in electron-positron collisions. We shall also study the beam polarization dependence of the background processes. The cross section with polarized $e^\pm$ beams, with polarization $P_{e^\pm}$ ($|P_{e^\pm}| \leq 1$), can be written as

$$\sigma(P_{e^-}, P_{e^+}) = 2\sum_\lambda\left(\frac{1 + P_{e^-}\lambda}{2}\right)\left(\frac{1 - P_{e^+}\lambda}{2}\right)\sigma_\lambda, \quad (4.1)$$

where σ_λ is the helicity dependent cross section, and where λ is the helicity ($\lambda = \pm 1$) of the initial particles ($e^\pm$). The signal radiative neutralino production cross section can be enhanced, and the background can be reduced by using a positively-polarized e^- beam ($P_{e^-} > 0$) and a negatively-polarized e^+ beam ($P_{e^+} < 0$).

In the NMSSM, and MSSM, the radiative neutralino production process proceeds mainly via the exchange of right selectrons $\tilde{e}_R$. This is because, for the parameter choices that we use, the neutralino has a significant bino component in these models, and the coupling to the right selectron is significantly larger as compared to the left selectrons $\tilde{e}_L$. This leads to the contribution from the right selectron exchange to the cross section which is an order of magnitude larger as compared to the left selectron exchange. Furthermore, compared to the right selectron exchange, the contribution from left selectron exchange is suppressed due to the fact that $m_{\tilde{e}_R} < m_{\tilde{e}_L}$. We also note that the Z boson exchange contribution to the neutralino production process is negligible in these models. The SM background radiative neutrino process proceeds mainly via the exchange of W bosons. This means that positive electron beam polarization P_{e^-} and negative positron beam polarization P_{e^+} will enhance the signal cross section, and at the same time reduce the background [39]. We note that $|P_{e^-}| > 0.8$ and $|P_{e^+}| > 0.5$ are designed at the International Linear Collider [65].

A quantitative measure of the excess of photons from the radiative neutralino production over the SM background photons is the theoretical significance defined as

$$S = \frac{N_S}{\sqrt{(N_S + N_B)}} = \frac{\sigma_S}{\sqrt{\sigma_S + \sigma_B}}\sqrt{\mathcal{L}}, \quad (4.2)$$

where N_S and N_B define the number of signal and background events, respectively, σ_S and σ_B are the respective cross sections, and $\mathcal{L}$ is the integrated luminosity. If the theoretical significance has a value $S = 1$ for a signal, then that signal can be measured at a 68% confidence level. In addition, we must also consider the signal to background ratio

$$r = \frac{\sigma_S}{\sigma_B}. \quad (4.3)$$

For a signal to be detectable at the International Linear Collider we must have $S > 1$ and $r > 1\%$. These estimates are expected to be rough estimates which will enable us to decide whether an excess of signal photons can be measured over the background photons. A detailed Monte Carlo analysis is beyond the scope of the present paper.

We have studied the radiative production of lightest neutralino for three different electron-positron center-of-mass energies, namely $\sqrt{s} = 350$ GeV, 500 GeV, and 650 GeV, respectively, with longitudinally polarized beams for the three models—MSSM SPS1a, MSSM EWSB and NMSSM using CALCHEP. For MSSM SPS 1a, we have calculated the beam polarization dependence of the signal cross section $\sigma(e^+e^- \to \tilde{\chi}_1^0\tilde{\chi}_1^0\gamma)$ and the background cross section $\sigma(e^+e^- \to \nu\bar{\nu}\gamma)$, the significance S and signal to background ratio r at $\sqrt{s} = 350$ GeV, 500 GeV and 650 GeV for the input parameters as in Table I. We report the values of cross sections $\sigma(e^+e^- \to \tilde{\chi}_1^0\tilde{\chi}_1^0\gamma)$ and $\sigma(e^+e^- \to \nu\bar{\nu}\gamma)$, S and r for a specific set of beam of polarizations $(P_{e^-}|P_{e^+}) = (0|0)$, $(0.8|0)$, $(0.8|-0.3)$, $(0.8|-0.6)$, $(0.9|0)$, $(0.9|-0.3)$, and $(0.9|-0.6)$ in Tables IV, V, and VI, respectively. We observe that there is a large enhancement in the value of $S = 106$ and $r = 50.4\%$ for $(P_{e^-}|P_{e^+}) = (0.9|-0.6)$ compared to all other chosen set of polarization values for $\sqrt{s} = 500$ GeV. For a previous study of the beam polarization effects for the radiative neutralino production in MSSM, see Ref. [66].

TABLE IV. Cross sections σ, significance S, and signal to background ratio r for different beam polarizations $(P_{e^-}|P_{e^+})$ for MSSM SPS 1a at $\sqrt{s} = 350$ GeV, with $\tan\beta = 10$ and $\mathcal{L} = 500$ fb^{-1}.

$(P_{e^-}\|P_{e^+})$	$(0\|0)$	$(0.8\|0)$	$(0.8\|-0.3)$	$(0.8\|-0.6)$	$(0.9\|0)$	$(0.9\|-0.3)$	$(0.9\|-0.6)$
$\sigma(e^+e^- \to \tilde{\chi}_1^0\tilde{\chi}_1^0\gamma)$	20 fb	35 fb	46 fb	56.4 fb	37 fb	48.4 fb	60 fb
$\sigma(e^+e^- \to \nu\bar{\nu}\gamma)$	2991 fb	793 fb	685 fb	579 fb	518 fb	501 fb	484 fb
S	8	27	38	50	35	46	57.5
r	0.7%	4.4%	6.7%	9.7%	7.1%	9.6%	12.4%

TABLE V. Cross sections σ, significance S, and signal to background ratio r for different beam polarizations $(P_{e^-}|P_{e^+})$ for MSSM SPS 1a at $\sqrt{s} = 500$ GeV, with $\tan\beta = 10$ and $\mathcal{L} = 500$ fb^{-1}.

$(P_{e^-}\|P_{e^+})$	$(0\|0)$	$(0.8\|0)$	$(0.8\|-0.3)$	$(0.8\|-0.6)$	$(0.9\|0)$	$(0.9\|-0.3)$	$(0.9\|-0.6)$
$\sigma(e^+e^- \to \tilde{\chi}_1^0\tilde{\chi}_1^0\gamma)$	23 fb	40 fb	52 fb	64 fb	42 fb	55 fb	67 fb
$\sigma(e^+e^- \to \nu\bar{\nu}\gamma)$	2942 fb	597 fb	423 fb	250 fb	304 fb	218 fb	133 fb
S	9.4	35.4	53.3	80.8	50.5	74.4	106
r	0.8%	6.7%	12.3%	25.6%	13.8%	25.2%	50.4%

TABLE VI. Cross sections σ, significance S, and signal to background ratio r for different beam polarizations $(P_{e^-}|P_{e^+})$ for MSSM SPS 1a at $\sqrt{s} = 650$ GeV, with $\tan\beta = 10$ and $\mathcal{L} = 500$ fb^{-1}.

$(P_{e^-}\|P_{e^+})$	$(0\|0)$	$(0.8\|0)$	$(0.8\|-0.3)$	$(0.8\|-0.6)$	$(0.9\|0)$	$(0.9\|-0.3)$	$(0.9\|-0.6)$
$\sigma(e^+e^- \to \tilde{\chi}_1^0\tilde{\chi}_1^0\gamma)$	18 fb	32 fb	42 fb	52 fb	34 fb	44 fb	55 fb
$\sigma(e^+e^- \to \nu\bar{\nu}\gamma)$	2869 fb	578 fb	408 fb	237 fb	292 fb	207 fb	123 fb
S	7.5	29	44	68	42	62	92
r	0.63%	5.5%	10.3%	22%	11.6%	21.3%	44.7%

TABLE VII. Cross sections σ, significance S, and signal to background ratio r for different beam polarizations $(P_{e^-}|P_{e^+})$ for MSSM EWSB at $\sqrt{s} = 350$ GeV, with $\tan\beta = 10$ and $\mathcal{L} = 500$ fb^{-1}.

$(P_{e^-}\|P_{e^+})$	$(0\|0)$	$(0.8\|0)$	$(0.8\|-0.3)$	$(0.8\|-0.6)$	$(0.9\|0)$	$(0.9\|-0.3)$	$(0.9\|-0.6)$
$\sigma(e^+e^- \to \tilde{\chi}_1^0\tilde{\chi}_1^0\gamma)$	1.7 fb	2.9 fb	3.8 fb	4.7 fb	3.1 fb	4 fb	4.p fb
$\sigma(e^+e^- \to \nu\bar{\nu}\gamma)$	2991 fb	793 fb	685 fb	579 fb	518 fb	501 fb	484 fb
S	0.7	2.3	3.2	4.3	3	4	5
r	0.06%	0.4%	0.56%	0.81%	0.6%	0.8%	1.02%

TABLE VIII. Cross sections σ, significance S, and signal to background ratio r for different beam polarizations $(P_{e^-}|P_{e^+})$ for MSSM EWSB at $\sqrt{s} = 500$ GeV, with $\tan\beta = 10$ and $\mathcal{L} = 500$ fb^{-1}.

$(P_{e^-}\|P_{e^+})$	$(0\|0)$	$(0.8\|0)$	$(0.8\|-0.3)$	$(0.8\|-0.6)$	$(0.9\|0)$	$(0.9\|-0.3)$	$(0.9\|-0.6)$
$\sigma(e^+e^- \to \tilde{\chi}_1^0\tilde{\chi}_1^0\gamma)$	2.2 fb	3.9 fb	5.1 fb	6.3 fb	4.1 fb	5.4 fb	6.6 fb
$\sigma(e^+e^- \to \nu\bar{\nu}\gamma)$	2942 fb	597 fb	423 fb	250 fb	804 fb	218 fb	133 fb
S	0.9	3.6	5.5	8.8	5.2	8	12.5
r	0.075%	0.65%	1.2%	2.5%	1.3%	2.5%	5%

Similarly, in the Tables VII, VIII, and IX, we discuss the values of cross sections $\sigma(e^+e^- \to \tilde{\chi}_1^0\tilde{\chi}_1^0\gamma)$ and $\sigma(e^+e^- \to \nu\bar{\nu}\gamma)$, S and r for a specific set of beam polarization values $(P_{e^-}|P_{e^+}) = (0|0)$, $(0.8|0)$, $(0.8|-0.3)$, $(0.8|-0.6)$, $(0.9|0)$, $(0.9|-0.3)$, and $(0.9|-0.6)$ for the case of MSSM EWSB. There is again a significant increase for the value of $S = 12.5$ and $r = 5\%$ for $(P_{e^-}|P_{e^+}) = (0.9|-0.6)$ compared to other chosen polarization values

TABLE IX. Cross sections σ, significance S, and signal to background ratio r for different beam polarizations $(P_{e^-}|P_{e^+})$ for MSSM EWSB at $\sqrt{s} = 650$ GeV, with $\tan\beta = 10$ and $\mathcal{L} = 500$ fb^{-1}.

$(P_{e^-}\|P_{e^+})$	(0|0)	(0.8|0)	(0.8| − 0.3)	(0.8| − 0.6)	(0.9|0)	(0.9| − 0.3)	(0.9| − 0.6)
$\sigma(e^+e^- \to \tilde{\chi}_1^0\tilde{\chi}_1^0\gamma)$	1.9 fb	3.4 fb	4.4 fb	5.4 fb	35 fb	4.6 fb	5.7 fb
$\sigma(e^+e^- \to \nu\bar{\nu}\gamma)$	2869 fb	578 fb	408 fb	237 fb	292 fb	207 fb	123 fb
S	0.8	3	4.8	7.7	4.5	7	11
r	0.06%	0.6%	1%	2.3%	1.2%	2.2%	4.6%

TABLE X. Cross sections σ, significance S, and signal to background ratio r for different beam polarizations $(P_{e^-}|P_{e^+})$ for NMSSM at $\sqrt{s} = 350$ GeV, with $\tan\beta = 10$ and $\mathcal{L} = 500$ fb^{-1}.

$(P_{e^-}\|P_{e^+})$	(0|0)	(0.8|0)	(0.8| − 0.3)	(0.8| − 0.6)	(0.9|0)	(0.9| − 0.3)	(0.9| − 0.6)
$\sigma(e^+e^- \to \tilde{\chi}_1^0\tilde{\chi}_1^0\gamma)$	1.1 fb	2 fb	2.6 fb	3.2 fb	2.1 fb	2.7 fb	3.3 fb
$\sigma(e^+e^- \to \nu\bar{\nu}\gamma)$	2991 fb	793 fb	685 fb	579 fb	518 fb	501 fb	484 fb
S	0.45	1.6	2.2	3	2	2.7	3.3
r	0.04%	0.25%	0.4%	0.55%	0.4%	0.54%	0.68%

TABLE XI. Cross sections σ, significance S, and signal to background ratio r for different beam polarizations $(P_{e^-}|P_{e^+})$ for NMSSM at $\sqrt{s} = 500$ GeV, with $\tan\beta = 10$ and $\mathcal{L} = 500$ fb^{-1}.

$(P_{e^-}\|P_{e^+})$	(0|0)	(0.8|0)	(0.8| − 0.3)	(0.8| − 0.6)	(0.9|0)	(0.9| − 0.3)	(0.9| − 0.6)
$\sigma(e^+e^- \to \tilde{\chi}_1^0\tilde{\chi}_1^0\gamma)$	1.2 fb	2.2 fb	2.8 fb	3.5 fb	2.3 fb	3 fb	3.7 fb
$\sigma(e^+e^- \to \nu\bar{\nu}\gamma)$	2942 fb	597 fb	423 fb	250 fb	804 fb	218 fb	133 fb
S	0.5	2	3	5	3	4.5	7
r	0.04%	0.4%	0.66%	1.4%	0.76%	1.4%	2.8%

TABLE XII. Cross sections σ, significance S, and signal to background ratio r for different beam polarizations $(P_{e^-}|P_{e^+})$ for NMSSM at $\sqrt{s} = 650$ GeV, with $\tan\beta = 10$ and $\mathcal{L} = 500$ fb^{-1}.

$(P_{e^-}\|P_{e^+})$	(0|0)	(0.8|0)	(0.8| − 0.3)	(0.8| − 0.6)	(0.9|0)	(0.9| − 0.3)	(0.9| − 0.6)
$\sigma(e^+e^- \to \tilde{\chi}_1^0\tilde{\chi}_1^0\gamma)$	1 fb	1.8 fb	2.3 fb	2.8 fb	1.9 fb	2.4 fb	3 fb
$\sigma(e^+e^- \to \nu\bar{\nu}\gamma)$	2869 fb	578 fb	408 fb	237 fb	292 fb	207 fb	123 fb
S	0.42	1.7	2.5	4	2.5	3.7	6
r	0.03%	0.3%	0.56%	1.2%	0.65%	1.16%	2.44%

TABLE XIII. Vertices corresponding to various terms in the interaction Lagrangian (A7) for MSSM. In addition we have also shown the vertices for selectron-photon and electron-photon interactions. The vertices for the NMSSM are obtained by replacing N_{ij} with N'_{ij}.

Vertex	Vertex factor
Right selectron—electron—neutralino	$\frac{-ie\sqrt{2}}{\cos\theta_w} N_{11}^* P_L$
Left selectron—electron—neutralino	$\frac{ie}{\sqrt{2}\sin\theta_w}(N_{12} + \tan\theta_w N_{11})P_R$
Neutralino—Z^0—neutralino	$\frac{ie}{4\sin\theta_w\cos\theta_w}(\|N_{13}\|^2 - \|N_{14}\|^2)\gamma^\mu\gamma^5$
Electron—Z^0—electron	$ie\gamma^\mu[\frac{1}{\sin\theta_w\cos\theta_w}(\frac{1}{2} - \sin^2\theta_w)P_L - \tan\theta_w P_R]$
Selectron—photon—selectron	$ie(p_1 + p_2)^\mu$
Electron—photon—electron	$ie\gamma^\mu$

for $\sqrt{s} = 500$ GeV. However, the enhancement is relatively small as compared to the MSSM SPS 1a scenario.

Finally, in Tables X, XI, and XII, we show the results for the case of NMSSM. We get the similar pattern but the value of $S = 7$ and $r = 2.8\%$ for $(P_{e^-}|P_{e^+}) = (0.9| - 0.6)$ is considerably smaller as compared to that of $S = 106$ and $r = 50.4\%$ in MSSM SPS 1a at $\sqrt{s} = 500$ GeV. Thus, if the radiative production of neutralinos is observed at a linear collider with polarized beams, then on the basis of the observed event rate it may be possible to distinguish between MSSM and NMSSM as the underlying low energy supersymmetric model.

V. SUMMARY AND CONCLUSIONS

The nonminimal supersymmetric standard model (NMSSM) solves μ problem of MSSM in an elegant manner and is, thus, an attractive alternative to the MSSM. We have carried out a detailed study of the radiative neutralino production process $e^+e^- \to \tilde{\chi}_1^0\tilde{\chi}_1^0\gamma$ in NMSSM for ILC energies, and compared the results with the corresponding results in the MSSM for both unpolarized and polarized e^- and e^+ beams. This process has a signature of a high energy photon and missing energy. We have obtained a typical set of parameter values for the NMSSM by imposing theoretical and experimental constraints on the parameter space of NMSSM. For the set of parameter values that we obtain in this manner, the lightest neutralino in NMSSM has a significant admixture of the fermionic component of the singlet chiral superfield S. Using this parameter set, we have studied in detail the radiative neutralino production cross section in NMSSM for the ILC energies for both unpolarized and polarized e^- and e^+ beams. For comparison with MSSM, we have used the MSSM SPS 1a and MSSM EWSB models. The background to this process comes from the SM process $e^+e^- \to \nu\bar{\nu}\gamma$, as well as the background from the supersymmetric process $e^+e^- \to \tilde{\nu}\tilde{\nu}^*\gamma$. All these processes have a signature of a highly energetic photon with missing energy. The photon energy distribution $d\sigma/dE_\gamma$, and the total cross section as a function of the total energy have been calculated for the NMSSM and for MSSM SPS 1a scenario at $\sqrt{s} = 500$ GeV using CALCHEP package. Because of the admixture of a singlet in the lightest neutralino, the cross section as a function of energy for the radiative neutralino production is lower in NMSSM than in MSSM. We have also studied the dependence of the cross section for radiative neutralino production on the $SU(2)_L$ gaugino mass parameter M_2 and the Higgs(ino) mass parameter μ, as well as its dependence on the selectron $(\tilde{e}_R, \tilde{e}_L)$ masses in NMSSM, and compared it with the corresponding results in MSSM. In order to quantify whether an excess of signal photons, N_S, can be measured over the background photons, N_B, from radiative neutrino production, we have analyzed the theoretical statistical significance $S = N_S/\sqrt{N_S + N_B}$. At the ILC, electron and positron beam polarizations can be used to significantly enhance the signal and suppress the background simultaneously. We have shown that the significance can then be increased almost by an order of magnitude, e.g. with $(P_{e^-}, P_{e^+}) = (0.8, -0.6)$ compared to $(P_{e^-}, P_{e^+}) = (0, 0)$. A possible feedback of ILC$_{500}$ results could motivate the immediate use of the low-luminosity option of the ILC at $\sqrt{s} = 650$ GeV in order to resolve model ambiguities between NMSSM and MSSM even at an early stage of the experiment and outline future search strategies at the upgraded ILC at 1 TeV. In our scenarios, the signal cross section for $(P_{e^-}|P_{e^+}) = (0.8| - 0.6)$ is larger than 3.5 fb, the significance $S > 5$, and the signal to background ratio is about $r > 1\%$. The background cross section can be reduced to 250 fb. Increasing the positron beam polarization to $P_{e^+} = -0.6$, both the signal cross section and the significance increase significantly. Thus the electron and positron beam polarization at the ILC are essential tools to observe radiative neutralino production.

ACKNOWLEDGMENTS

P. N. P. would like to thank The Institute of Mathematical Sciences, India for hospitality where this work was initiated. The work of P. N. P. is supported by the Council of Scientific and Industrial Research, and by the J. C. Bose National Programme of the Department of Science and Technology, India. India. P. N. P. would like to thank the Inter University Centre for Astronomy and Astrophysics for hospitality while this work was being completed.

APPENDIX A: SUPERPOTENTIAL, NEUTRALINO MASS MATRIX AND COUPLINGS

For completeness we summarize here the couplings of the neutralinos to electrons and the scalar partners of electrons, the selectrons, in MSSM and in NMSSM. These couplings can be obtained from the neutralino mixing matrix. To obtain the neutralino mixing matrix for the MSSM, we recall that the neutralino mass matrix obtains contributions from part of the MSSM superpotential

$$W_{\rm MSSM} = \mu H_1 H_2, \tag{A1}$$

where H_1 and H_2 are the two Higgs doublet chiral superfields, and μ is the supersymmetric Higgs(ino) parameter. In addition to the contribution from the superpotential, the neutralino mass matrix receives contributions from the interactions between gauge and matter multiplets, as well as contributions from the soft supersymmetry breaking masses for the gauginos. Including all these contributions, the neutralino mass matrix, in the bino, wino, Higgsino basis $(-i\lambda', -i\lambda^3, \psi_{H_1}^1, \psi_{H_2}^2)$ can be written as [51,52]

$$M_{\rm MSSM} = \begin{pmatrix} M_1 & 0 & -m_Z\sin\theta_w\cos\beta & m_Z\sin\theta_w\sin\beta \\ 0 & M_2 & m_Z\cos\theta_w\cos\beta & -m_Z\cos\theta_w\sin\beta \\ -m_Z\sin\theta_w\cos\beta & m_Z\cos\theta_w\cos\beta & 0 & -\mu \\ m_Z\sin\theta_w\sin\beta & -m_Z\cos\theta_w\sin\beta & -\mu & 0 \end{pmatrix}, \tag{A2}$$

where M_1 and M_2 are the $U(1)_Y$ and the $SU(2)_L$ soft supersymmetry breaking gaugino mass parameters, respectively, and $\tan\beta = v_2/v_1$ is the ratio of the vacuum expectation values of the neutral components of the two Higgs doublet fields H_1 and H_2, respectively. Furthermore, m_Z is the Z boson mass, and θ_w is the weak mixing angle. We shall assume that all the parameters in the matrix M are real, in which case M is a real symmetric matrix and can be diagonalized by an orthogonal matrix. If one of the eigenvalues of M is negative, one can diagonalize this matrix using a unitary matrix N, the neutralino mixing matrix, to get a positive diagonal matrix [51]:

$$N^* M_{\rm MSSM} N^{-1} = {\rm diag}(m_{\chi_1^0}, m_{\chi_2^0}, m_{\chi_3^0}, m_{\chi_4^0}). \tag{A3}$$

where $m_{\chi_i^0}(i = 1, 2, 3, 4)$ are neutralino masses arranged in order of increasing value.

For the NMSSM, the relevant part of the superpotential is

$$W_{\rm NMSSM} = \lambda S H_1 H_2 - \frac{\kappa}{3} S^3, \tag{A4}$$

where S is the Higgs singlet chiral superfield. In the basis $(-i\lambda', -i\lambda^3, \psi^1_{H_1}, \psi^2_{H_2}, \psi_S)$, the neutralino mass matrix for the NMSSM can then be written as [24,25]

$$M_{\rm NMSSM} = \begin{pmatrix} M_1 & 0 & -m_Z\sin\theta_w\cos\beta & m_Z\sin\theta_w\sin\beta & 0 \\ 0 & M_2 & m_Z\cos\theta_w\cos\beta & -m_Z\cos\theta_w\sin\beta & 0 \\ -m_Z\sin\theta_w\cos\beta & m_Z\cos\theta_w\cos\beta & 0 & -\lambda x & -\lambda v_2 \\ m_Z\sin\theta_w\sin\beta & -m_Z\cos\theta_w\sin\beta & -\lambda x & 0 & -\lambda v_1 \\ 0 & 0 & -\lambda v_2 & -\lambda v_1 & 2\kappa x \end{pmatrix}, \tag{A5}$$

where $\langle S\rangle = x$ is the vacuum expectation value of the singlet Higgs field. As in the case of MSSM, we can use a unitary matrix N' to get a positive semidefinite diagonal matrix with the neutralino masses $m_{\chi_i^0}(i = 1, 2, 3, 4, 5)$ [24,25]:

$$N'^* M_{\rm NMSSM} N'^{-1} = {\rm diag}(m_{\chi_1^0}, m_{\chi_2^0}, m_{\chi_3^0}, m_{\chi_4^0}, m_{\chi_5^0}). \tag{A.6}$$

The Lagrangian for the interaction of neutralinos, electrons, selectrons and Z bosons for MSSM is given by [51]

$$\begin{aligned} \mathcal{L} = {} & \left(-\frac{\sqrt{2}e}{\cos\theta_w} N_{11}^*\right)\bar{f}_e P_L \tilde{\chi}_1^0 \tilde{e}_R + \frac{e}{\sqrt{2}\sin\theta_w}(N_{12} + \tan\theta_w N_{11})\bar{f}_e P_R \tilde{\chi}_1^0 \tilde{e}_L + \frac{e}{4\sin\theta_w\cos\theta_w}(|N_{13}|^2 \\ & - |N_{14}|^2) Z_\mu \bar{\tilde{\chi}}_1^0 \gamma^\mu \gamma^5 \tilde{\chi}_1^0 + e Z_\mu \bar{f}_e \gamma^\mu \left[\frac{1}{\sin\theta_w\cos\theta_w}\left(\frac{1}{2} - \sin^2\theta_w\right) P_L - \tan\theta_w P_R\right] f_e + {\rm H.c.}, \end{aligned} \tag{A7}$$

with the electron, selectron, neutralino and Z boson fields denoted by f_e, $\tilde{e}_{L,R}$, $\tilde{\chi}_1^0$, and Z_μ, respectively, and $P_{R,L} = \frac{1}{2} \times (1 \pm \gamma^5)$. The corresponding interaction Lagrangian for NMSSM is obtained from (A7) by replacing N_{ij} with N'_{ij}. The different vertices following from (A7) are shown in Table XIII. The couplings of the lightest neutralino to electrons, selectrons and Z boson are determined by the corresponding elements of the neutralino mixing matrix (N_{ij} or N'_{ij}).

[1] J. Wess and J. Bagger, *Supersymmetry and Supergravity* (Princeton University Press, Princeton, NJ, 1992), p. 259.

[2] G. 't Hooft, in *Recent Developments in Gauge Theories. Proceedings, Nato Advanced Study Institute, Cargese, France, 1979*, Nato Advanced Study Institutes Series: Series B, Physics Vol. 59 (Plenum, New York, 1980), p. 438; E. Witten, Nucl. Phys. **B188**, 513 (1981); R. K. Kaul, Phys. Lett. **109B**, 19 (1982); R. K. Kaul and P. Majumdar, Nucl. Phys. **B199**, 36 (1982); R. K. Kaul, Pramana **19**, 183 (1982).

[3] H. P. Nilles, Phys. Rep. **110**, 1 (1984).

[4] M. Drees, R. Godbole, and P. Roy, *Theory and Phenomenology of Sparticles: An Account of Four-Dimensional N = 1 Supersymmetry in High Energy Physics* (World Scientific, Hackensack, NJ, 2004), p. 555.

[5] J. A. Aguilar-Saavedra *et al.* (ECFA/DESY LC Physics Working Group), arXiv:hep-ph/0106315.

[6] T. Abe *et al.* (American Linear Collider Working Group), in *Linear Collider Physics Resource Book for Snowmass 2001. 1: Introduction*, edited by N. Graf, Proc. of the APS/

DPF/DPB Summer Study on the Future of Particle Physics (unpublished).

[7] K. Abe *et al.* (ACFA Linear Collider Working Group), arXiv:hep-ph/0109166.

[8] G. Weiglein *et al.* (LHC/LC Study Group), Phys. Rep. **426**. 47 (2006).

[9] J. A. Aguilar-Saavedra *et al.*, Eur. Phys. J. C **46**, 43 (2006).

[10] G. A. Moortgat-Pick *et al.*, Phys. Rep. **460**. 131 (2008).

[11] P. Fayet, Nucl. Phys. **B90**, 104 (1975); H. P. Nilles, M. Srednicki, and D. Wyler, Phys. Lett. **120B**, 346 (1983); J. P. Derendinger and C. A. Savoy, Nucl. Phys. **B237**, 307 (1984).

[12] J. R. Ellis, J. F. Gunion, H. E. Haber, L. Roszkowski, and F. Zwirner, Phys. Rev. D **39**, 844 (1989).

[13] M. Drees, Int. J. Mod. Phys. A **4**, 3635 (1989).

[14] P. N. Pandita, Phys. Lett. B **318**, 338 (1993); Z. Phys. C **59**, 575 (1993); U. Ellwanger, Phys. Lett. B **303**, 271 (1993); U. Ellwanger, M. Rausch de Traubenberg, and C. A. Savoy, Phys. Lett. B **315**, 331 (1993); S. F. King and P. L. White, Phys. Rev. D **53**, 4049 (1996).

[15] B. Ananthanarayan and P. N. Pandita, Int. J. Mod. Phys. A **12**, 2321 (1997).

[16] B. Ananthanarayan and P. N. Pandita, Phys. Lett. B **371**, 245 (1996).

[17] B. Ananthanarayan and P. N. Pandita, Phys. Lett. B **353**, 70 (1995).

[18] M. Chemtob and P. N. Pandita, Phys. Rev. D **73**, 055012 (2006).

[19] M. Chemtob and P. N. Pandita, Phys. Rev. D **76**, 095019 (2007).

[20] For a review and references, see e.g. U. Ellwanger, C. Hugonie, and A. M. Teixeira, Phys. Rep. **496**, 1 (2010).

[21] U. Ellwanger, J. F. Gunion, and C. Hugonie, J. High Energy Phys. 07 (2005) 041.

[22] G. A. Moortgat-Pick, S. Hesselbach, F. Franke, and H. Fraas, in *The Proceedings of 2005 International Linear Collider Workshop (LCWS 2005), Stanford, California,*, eConf C050318 (2005), p. 0206.

[23] J. F. Gunion, D. Hooper, and B. McElrath, Phys. Rev. D **73**, 015011 (2006).

[24] P. N. Pandita, Phys. Rev. D **50**, 571 (1994).

[25] P. N. Pandita, Z. Phys. C **63**, 659 (1994).

[26] S. Y. Choi, D. J. Miller, and P. M. Zerwas, Nucl. Phys. B **711**, 83 (2005).

[27] H. Goldberg, Phys. Rev. Lett. **50**, 1419 (1983).

[28] J. R. Ellis, J. S. Hagelin, D. V. Nanopoulos, K. A. Olive, and M. Srednicki, Nucl. Phys. **B238**, 453 (1984).

[29] A. Bartl, H. Fraas, and W. Majerotto, Nucl. Phys. **B278**, 1 (1986).

[30] J. R. Ellis, J. M. Frere, J. S. Hagelin, G. L. Kane, and S. T. Petcov, Phys. Lett. **132B**, 436 (1983); E. Reya, Phys. Lett. **133B**, 245 (1983); P. Chiappetta, J. Soffer, P. Taxil, F. M. Renard, and P. Sorba, Nucl. Phys. **B262**, 495 (1985),.**B279**, 824(E) (1987).

[31] P. Fayet, Phys. Lett. **117B**, 460 (1982).

[32] J. R. Ellis and J. S. Hagelin, Phys. Lett. **122B**, 303 (1983).

[33] K. Grassie and P. N. Pandita, Phys. Rev. D **30**, 22 (1984).

[34] T. Kobayashi and M. Kuroda, Phys. Lett. **139B**, 208 (1984).

[35] J. D. Ware and M. E. Machacek, Phys. Lett. **142B**, 300 (1984).

[36] L. Bento, J. C. Romao, and A. Barroso, Phys. Rev. D **33**, 1488 (1986).

[37] M. Chen, C. Dionisi, M. Martinez, and X. Tata, Phys. Rep. **159**, 201 (1988).

[38] T. Kon, Prog. Theor. Phys. **79**, 1006 (1988).

[39] S. Y. Choi, J. S. Shim, H. S. Song, J. Song, and C. Yu, Phys. Rev. D **60**, 013007 (1999).

[40] A. Datta, A. Datta, and S. Raychaudhuri, Eur. Phys. J. C **1**, 375 (1998); A. Datta, A. Datta, and S. Raychaudhuri, Phys. Lett. B **349**, 113 (1995).

[41] S. Ambrosanio, B. Mele, G. Montagna, O. Nicrosini, and F. Piccinini, Nucl. Phys. **B478**, 46 (1996).

[42] A. Heister *et al.* (ALEPH Collaboration), Eur. Phys. J. C **28**, 1 (2003).

[43] J. Abdallah *et al.* (DELPHI Collaboration), Eur. Phys. J. C **38**, 395 (2005).

[44] P. Achard *et al.* (L3 Collaboration), Phys. Lett. B **587**, 16 (2004).

[45] G. Abbiendi *et al.* (OPAL Collaboration), Eur. Phys. J. C **29**, 479 (2003).

[46] G. Abbiendi *et al.* (OPAL Collaboration), Eur. Phys. J. C **18**, 253 (2000).

[47] K. J. F. Gaemers, R. Gastmans, and F. M. Renard, Phys. Rev. D **19**, 1605 (1979).

[48] M. Gataullin (LEP Collaboration), Eur. Phys. J. C **33**, s791 (2003).

[49] H. K. Dreiner, O. Kittel, and U. Langenfeld, Phys. Rev. D **74**, 115010 (2006).

[50] R. Basu, P. N. Pandita, and C. Sharma, Phys. Rev. D **77**, 115009 (2008).

[51] H. E. Haber and G. L. Kane, Phys. Rep. **117**, 75 (1985).

[52] A. Bartl, H. Fraas, W. Majerotto, and N. Oshimo, Phys. Rev. D **40**, 1594 (1989).

[53] B. C. Allanach *et al.*, in *Proceedings of the APS/DPF/DPB Summer Study on the Future of Particle Physics* edited by N. Graf (unpublished); Eur. Phys. J. C **25**, 113 (2002); 125 (2001).

[54] A. Pukhov, arXiv:hep-ph/0412191.

[55] S. Eidelman *et al.* (Particle Data Group), Phys. Lett. B **592**, 1 (2004).

[56] F. A. Berends, G. J. H. Burgers, C. Mana, M. Martinez, and W. L. van Neerven, Nucl. Phys. **B301**, 583 (1988).

[57] F. Boudjema *et al.*, in *Geneva 1995, Physics at LEP2*, edited by G. Altarelli, T. Sjostrand, and F. Zwirner, Vol. 1, p. 207 (unpublished).

[58] G. Montagna, M. Moretti, O. Nicrosini, and F. Piccinini, Nucl. Phys. **B541**, 31 (1999).

[59] F. Franke and H. Fraas, Phys. Rev. D **49**, 3126 (1994).

[60] N. Ghodbane and H. U. Martyn, in *Proceedings of the APS/DPF/DPB Summer Study on the Future of Particle Physics*, edited by N. Graf (unpublished).

[61] H. E. Haber and D. Wyler, Nucl. Phys. **B323**, 267 (1989).

[62] S. Ambrosanio and B. Mele, Phys. Rev. D **53**, 2541 (1996).

[63] S. Ambrosanio and B. Mele, Phys. Rev. D **55**, 1399 (1997); **56**, 3157 (1997).

[64] H. Baer and T. Krupovnickas, J. High Energy Phys. 09 (2002) 038.

[65] J. Brau *et al.* (ILC Collaboration), arXiv:0712.1950.

[66] H. K. Dreiner, O. Kittel, and U. Langenfeld, Eur. Phys. J. C **54**, 277 (2008).